SIM Narrow and wide angle astrometric demonstration on the MAM testbed.

Renaud Goullioud*, Tsae-Pyng J. Shen, Joseph H. Catanzarite,
Jet Propulsion Laboratory, California Institute of Technology,
4800 Oak Grove Dr, Pasadena, CA, USA 91109

ABSTRACT

The Space Interferometry Mission (SIM) requires fringe measurements to the level of picometers in order to produce astrometric data at the micro-arc-second level. To be more specific, it is necessary to measure both the position of the starlight central fringe and the change in the internal optical path of the interferometer to tens of picometers. The internal path is measured with a small heterodyne metrology beam, whereas the starlight fringe position is estimated with a CCD sampling a large concentric annular beam. One major challenge for SIM is to align the metrology beam with the starlight beam to keep the consistency between these two sensors at the system level while articulating the instrument optics over the field of regard.

The Micro-Arcsecond Metrology testbed (MAM), developed at the Jet Propulsion Laboratory, features an optical interferometer with a white light source, all major optical components of a stellar interferometer and heterodyne metrology sensors. The setup is installed inside a large vacuum chamber in order to mitigate the atmospheric and thermal disturbances. Astrometric observations are simulated by articulating the optics over the 15 degrees field of regard to generate multiple artificial stars. Recent data show agreement between the metrology and starlight paths to 20pm in the narrow angle field and to 350pm in the full wide angle field of regard of SIM. This paper describes the MAM optical setup, the observation process, the current data and how the performance relates to SIM.

1. INTRODUCTION

The MAM experiment is a key ground-based testbed that will demonstrate some critical technologies for SIM, the Space Interferometry Mission. SIM is a space-based Michelson interferometer that will carry out astrometry to micro-arcsecond precision on the visible light from a large sample of stars in our galaxy [1]. SIM has a daunting list of technological challenges to address in order to show the mission is technically achievable. These challenges range from nanometer control problems to picometer sensing problems. Several system-level testbeds have been designed, built, and tested thus far in SIM's evolution. Each testbed is intended to address a system-level aspect of the SIM technology challenge. Examples of such testbeds include the Micro-Precision Interferometer testbed [2], the SIM Testbed 3 [3,4], and the KITE testbed [5].

Interferometry of such high precision requires extremely accurate knowledge of optical path length changes, and hence extremely precise internal metrology. For SIM to succeed, the optical pathlength metric provided by the interferometer fringe determination must be faithfully consistent, at the level of tens of picometers, with the distances measured by metrology gauges, through all the operational motions of interferometer delay line and siderostats. The purpose of MAM is to demonstrate this agreement in a large-scale simulation that implements a substantial fraction of the final SIM flight functionality.

Two distinct modes of astrometry will be implemented on SIM: narrow and wide angles. For the narrow angle astrometry, SIM will perform measurements of the position of a target star relative to a set of reference stars within a one-degree field, with an accuracy of 1 micro-arcsecond at each visit [6]. In contrast, for the wide angle astrometry, SIM will perform measurements of the global position of target stars by tying together 15-degree tiles using grid stars. This

* renaud@jpl.nasa.gov; phone: (1) 818 354 7908

effort will take several years but will eventually reach a global accuracy of 4 micro-arcseconds. The demonstration of the observation of the target stars within a given tile is the main objective of this paper.

Fig. 1 is a picture of the MAM experiment in the 45 foot long vacuum chamber that provides the vacuum necessary to obtain the required sub-nanometer performance. Fig. 2 shows a schematic optical layout of the MAM experiment. MAM naturally divides into two distinct subsystems: the Test Article (TA), which is the interferometer proper, and the Inverse Interferometer Pseudo-Star (IIPS). The pseudo-star emulates a distant target star by providing spatially coherent wavefronts out of two mirrors, separated by 1.5 meters, that feed directly into the two siderostats of TA. The two feed mirrors of IIPS are articulated (in translation and tilt) in order to simulate stars located at different orientations in space while still illuminating the TA siderostats.

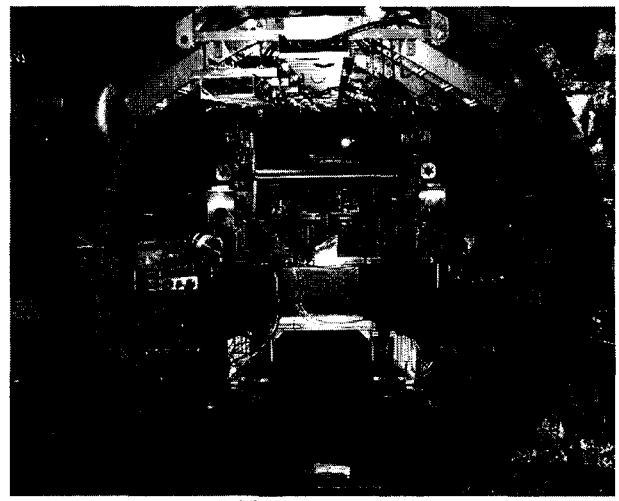

Fig. 1. The MAM experiment.

The central main beam combiner on the TA side is the beam splitter at which light from the two arms of the interferometer are brought together to produce interference. TA also contains a CCD camera to record fringes, a delay line to adjust the optical pathlength difference (OPD) between the two arms of the interferometer, and a voice-coil modulator to scan the OPD for fringe detection.

The conceptual dividing line between TA and IIPS is at the vertices of the two small corner cubes that are located within the sub-apertures of the two siderostats in TA. Metrology gauge launchers in both TA and IIPS sides measure round-trip distances, with precision in the neighborhood of 10 pm, to and from the vertices of these corner cubes. In this way, the complete optical path traversed by starlight is measured by metrology, in two pieces.

A severe technical constraint on the problem of tracking interferometric fringes with metrology sensors to picometer precision is faced by MAM as it will be by SIM. The starlight signal measured by the interferometer travels in a 40 mm annular beam that fills a large portion of the siderostats, while the laser light for metrology travels in small pencil beams located within the "sub-aperture", or obscured 18 mm center of these annuli, where they are directed to the reference corner cubes at the centers of the siderostats. The great difference in optical footprint of interferometry and metrology beams puts a premium on accurate optical alignment.

Some of technical details of MAM are discussed next, while more detailed information can be found in reference [7].

2. TESTBED DESCRIPTION

2.1. Inverse Interferometer Pseudo-Star

The starlight beam emerges in the IIPS source with a beam pattern typical of launching into free space from a bare fiber (Fig. 2). The spectrum of the 600-1000 nm white light ("starlight") corresponds to a blackbody at a temperature of about

3100 K. In addition to the white light source, IIPS contains a number of auxiliary light sources that are used as beacons for alignment and calibration of system [7].

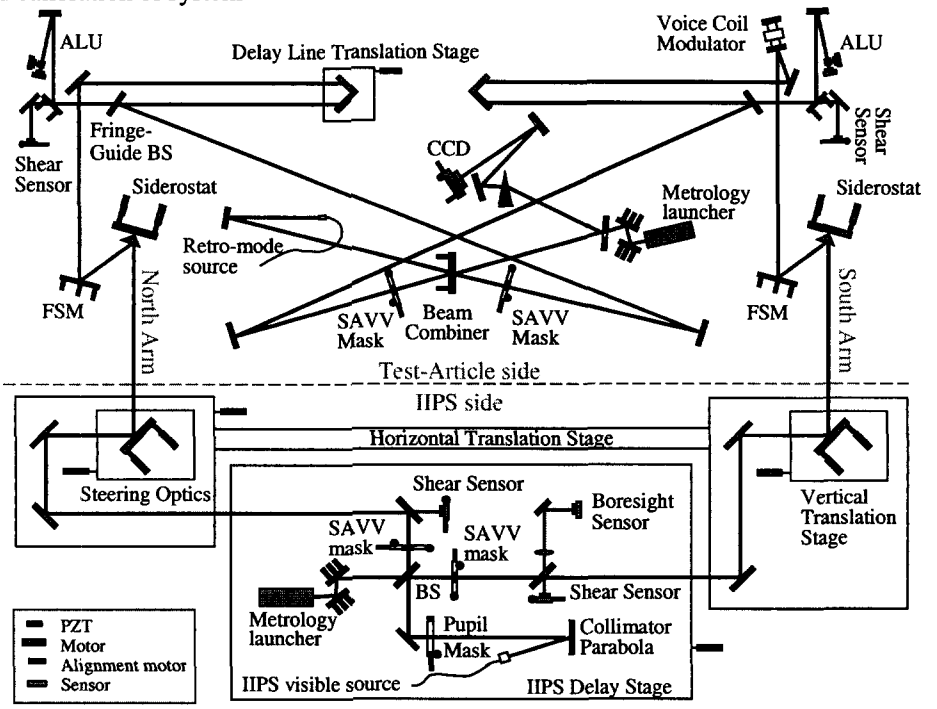

Fig. 2. MAM main optical layout.

The visible starlight is then collimated by a paraboloid (Fig. 2) before being directed to the main beam splitter (BS) that will divide the beam for the two output arms of IIPS. The starlight beams are sent from two IIPS steering mirrors directly opposite TA's two siderostats. To accommodate motions of the siderostats that emulate observations of multiple stars at different field positions, the IIPS steering mirrors are mounted on translation stages whose motions are determined as part of the alignment procedure.

2.2. Metrology Detector

Heterodyne detection for metrology is done within the two independent launchers, one on the TA and one on the IIPS side of MAM in Fig. 2. Each launcher sends out two independent sets of dual measurement beams that traverse the two arms of TA or IIPS, where they are ultimately retro-reflected on the two siderostats. The roundtrip distance is measured by heterodyne interferometry against a reference beam (local oscillator) that is kept physically confined within each launcher [8].

2.3. Delay Line and Voice Coil Modulator

The corner-cube delay line is used to balance the two arms in order to find the white light fringes. Reference [9] describes in details the pathlength control and the actuator design. The delay line consists of a large corner cube mounted on top of a precision motorized translation stage. Using a corner cube as a delay line preserves the optical beam orientation when slewing along the track.

The voice coil modulator scans the path by one micron at 25 Hz in order to solve for the starlight fringe phase with the CCD. It is also used for pathlength control to reduce the errors due to OPD jitter at the recombination. The voice coil modulator consists of a flat mirror mounted on one side of a flexure and a voice coil mounted on the opposite side. A magnet is mounted to the housing of the assembly. The voice coil actuator provides pure motion of the mirror in piston.

2.4. Siderostats

A fundamental actuation in MAM is the motion of the siderostats to simulate observations of multiple stellar targets by SIM. Fig. 3 shows one of the two siderostats. The siderostat motors control gross pointing, while piezo actuators carry out high-bandwidth tip-tilt corrections to lock the peak of the starlight signal onto a certain position on the CCD.

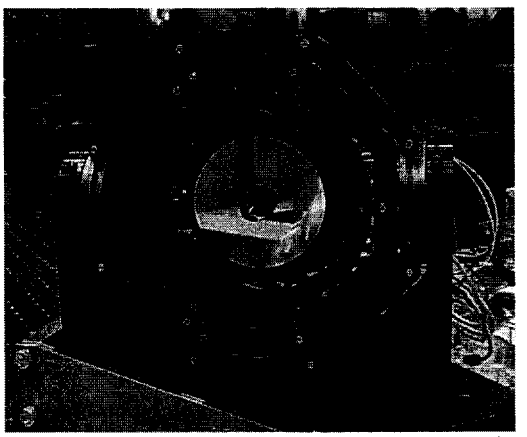

Fig. 3. MAM siderostat with corner-cube at the center of the optics.

Because the corner cube at the center of the siderostat mirror has its vertex very close to the intersection of the gimbal axes, the siderostat can be moved without affecting the OPD measured by the metrology beams. The collocation of the corner-cube vertex, the siderostat mirror and the gimbal axis is a key driver of the siderostat design. The corner-cube vertex to mirror offset was measured to be less than 0.5 microns [10].

2.5. Alignment Sensors and Actuators

A number of sensors have been built into MAM specifically to monitor optical alignment, and a number of actuators have been implemented to make the adjustments to the alignment that are indicated by the readings of those sensors. These detectors generally measure either tip/tilt or beam shear; these may be accomplished with quadrant photo-detectors at the focal plane or at the pupil plane, respectively. MAM must be operated in a vacuum chamber to minimize the large errors induced by atmospheric turbulence, so remote motorized control of the many adjustable subsystems is required. Fig. 2 gives a schematic indication of the motors that drive some of the key actuators. Reference [7] presents a detailed description of the alignment sensors and how the precise alignment is obtained.

2.6. White Light Detection

White light fringes are detected by modulating the optical path in a triangle wave pattern [9]. The central sensor is the CCD camera, a small-format (40x40) silicon device used to monitor fringe intensity from the white-light beam as the interferometer optical path difference is scanned about one micron. MAM has the ability to measure the positions of the modulation waveform at picometer accuracy by internal metrology at a 1 kHz rate. The fringe intensity data is recorded on the CCD camera at 500 frames/second. For a 25 Hz triangle waveform, we record 20 CCD frames during one triangle waveform. We average samples of metrology data to match the camera data.

White light fringes are spectrally dispersed linearly in wave number by the dispersion prism ("spectrometer") onto the CCD camera. A single recorded frame from a 40x3 sub-region of the 40x40 camera is shown in Fig. 4. White light is dispersed nearly uniformly between the 16^{th} (710 nm) through 40^{th} (950 nm) pixels, and HeNe laser light is also centered at left on the 4th pixel.

For each recorded CCD frame, we co-add the recorded intensity of three rows at each pixel for analysis. Each white light pixel covers between 7 nm to 11 nm of spectral width, and hence can be fit for quasi-monochromatic fringes [6]. A new fringe-phase measurement is produced every 40 ms for the voice-coil modulator scanning at 25 Hz. A typical fringe from a given CCD pixel and its corresponding dither positions from metrology are shown in Fig. 5. Vibrations, drifts, detector noise, all will appear in the recorded fringes and hence limit the accuracy in phase delay estimation. The relative phase between white light and metrology is the quantity of interest for all subsequent data analysis.

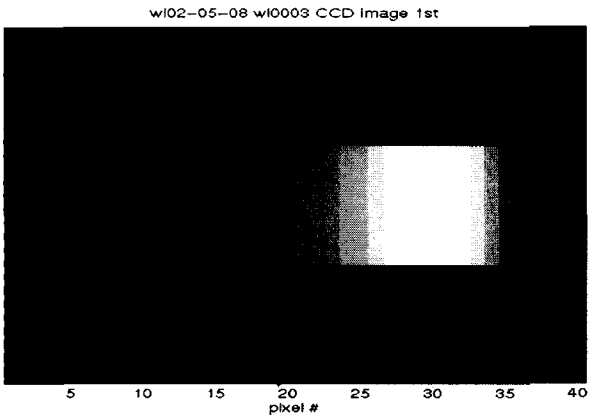

Fig. 4. Dispersed fringe image on the camera.

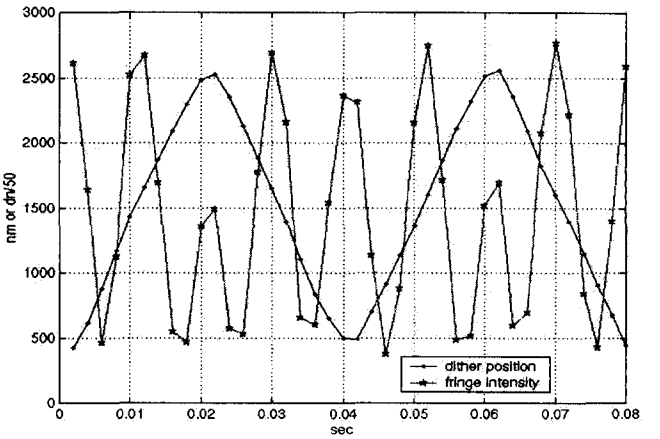

Fig. 5. Actual fringe and dither positions observed in MAM testbed.

3. ASTROMETRIC EXPERIMENTS ON MAM

3.1. Field Dependency of the Errors

Errors in the difference between the starlight and metrology on SIM's interferometers can be divided into two major categories: field independent and field dependent:

- Field independent errors are the same no matter where the SIM is "looking" in the field, i.e. where the collecting apertures or the delay line resides. Examples of field independent errors are photon noise on a camera or thermal expansion causing misalignment. Field independent errors are mostly of two time scales: fast random or slow drift. Averaging reduces the random error whereas drift errors can be estimated by repeating the same reference star measurement several times during the experiment.
- Field dependent errors change as a function of location of the articulating collecting apertures and/or translating delay lines. An example is diffraction that affects the starlight and metrology differently as the delay line translates on its rails. This difference shows up as an error in the relative delay determination. However, it is possible to remove this error through calibration. Without calibration, it would be impossible for SIM to tell the difference between the desired astrometric delay and field dependent errors.

3.2. MAM versus SIM Basics

SIM uses metrology to measure the difference between starlight and metrology in order to determine how much further the starlight traveled to one aperture than to the other. The metrology goes only through the test article optics. In the case of MAM however, the metrology goes through the entire test article, and continues all the way to the pseudo-star. SIM's starlight versus metrology difference signal contains the astrometric delay (the value of interest), field independent and field dependent. In contrast, MAM's starlight versus metrology difference signal contains the field independent and field dependent errors of both the pseudo-star and the test article, but no astrometric delay. This in fact leads to the fundamental rule of MAM: MAM measures directly the field dependent function for the combined pseudo-star / test article system.

3.3. Wide angle scenario

The goal of the wide angle experiments is to quantify the random errors and residual field-dependent errors on MAM instrument measurements of white-light minus metrology over a wide angle field of regard. We also want to make the procedure as close as possible to what will be done on the SIM flight system.

Data for wide angle tests are gathered from target star positions arranged over a square grid that essentially fills a circular field of 15° in diameter. A variety of grid scan patterns, called "sequences", have been tried; an example is shown in Fig. 6. X is parallel to the baseline of the interferometer, so it is the direction along which the delay line moves; Y is perpendicular to the direction of the motion of the delay line.

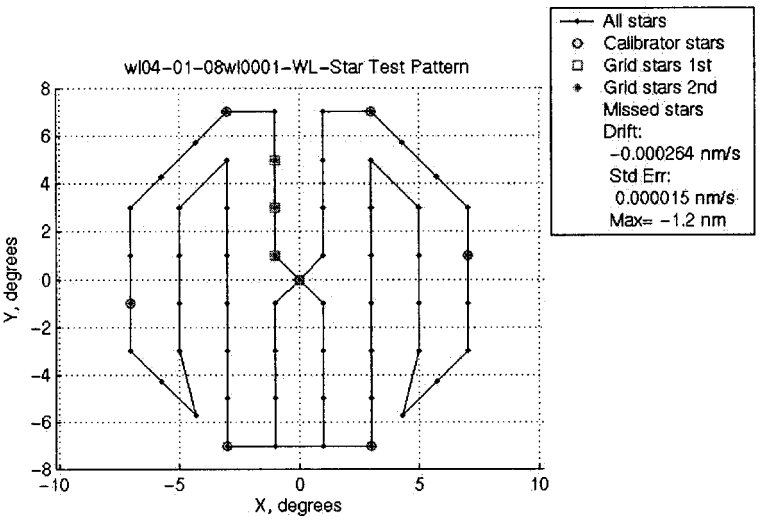

Fig. 6 Wide angle sequence grid pattern covering the 15° field of regard (vertical scan).

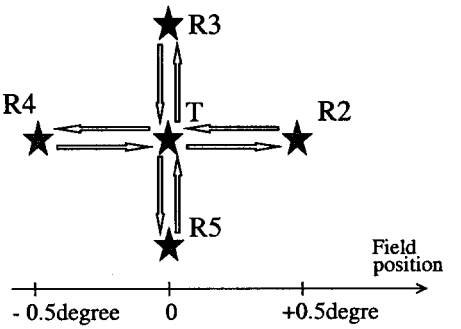

Figure 7 Narrow angle chopping sequence covering a one-degree filed of regard.

3.4. Wide Angle Calibration

The SIM on-orbit observation scenario includes some field dependent calibration function measurement. This function is then used to compensate for the field dependent errors on each of the measurements. In the SIM mission, delay measurements on stars in a tile are fit simultaneously for star positions and baseline length and orientation, as well as a constant bias offset term for the tile. Errors in the delay measurements on SIM derive from:

- constant bias offset due to metrology tracking,
- knowledge errors in catalog star positions,
- knowledge errors in baseline orientation and length,
- field-dependent errors due to articulation of optical elements,
- time-dependent drift due to thermal and other effects.

MAM measurements will be subject to all these errors except for knowledge errors in star positions.

The combined errors due to uncertainty in knowledge of the baseline and uncertainty in knowledge of the static bias offset are effectively indistinguishable from field-dependent errors of the following form:

$$E(X,Y) = a + bX + cY + d(X^2 + Y^2) \quad (1)$$

where X and Y are Cartesian position coordinates of the star (in terms of delays) and a, b, c, and d are static calibration constants. SIM data processing will use a set of grid stars in each tile to solve for a, b, c, and d values.

3.5. Wide Angle Data Acquisition Procedure

Our approach matches the SIM scenario. It uses a set of seven 'calibration stars' to fit the MAM delay measurements to a field dependent model of the form of Eq. 1. Subtracting the fitted model from the delay data effectively removes errors of this form. The residuals will contain a systematic component of higher-order field-dependent terms as well as random error. The MAM wide angle measurements of white-light minus metrology delays can be decomposed by the following equation:

$$D_{Raw}(X_i,Y_i,T_i) = a + bX_i + cY_i + d(X_i^2+Y_i^2) + hT_i + \varepsilon_i \quad (2)$$

where D_{Raw} is the difference between the MAM white-light and metrology delay measurements of the optical path with the pseudo-star at the i'th field position in the sequence; X_i and Y_i are the Cartesian coordinates of the pseudo-star position; T_i is the time at the midpoint of the delay measurement; h is the slope of the linear time-dependent drift; ε_i is

the residual error, which contains higher order field-dependence, nonlinear time drift, random error, and possibly other systematic components.

The top-level single interferometer performance number derived from the SIM wide angle requirement tree is 280 pm. It maps to a 4 micro-arcsecond performance over 5 years of mission.

3.6. Narrow angle scenario

The measurement represents a single SIM narrow angle observation. The definition of a SIM measurement as defined in the SIM error budget involves observing a target star (one suspected of having orbiting planets) for 300 seconds, slewing to one or more local reference stars, and observing them for 300 seconds total. The desired quantity is the difference in delays between the target star and the reference star(s).

The integration time per observation for both the reference and the target is limited in order to support the science demands for the entire mission. It is however possible to interleave the reference and target observations in order to remove instrument drift errors. This observing sequence is called "chopping".

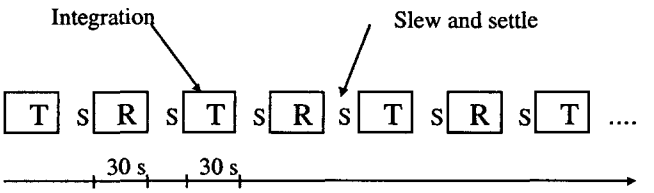

The chop time should be long enough to minimize random errors and short compared to the drift time constant in order to remove drift contributions effectively. The number of allowed chops is determined by the chosen chop time and allowable 300 second total integration time. The current chop scenario is ten 30 second chops.

For the field dependent tests, the sequence involves moving to multiple field points, recording the difference between starlight and metrology through the entire path of MAM for 30 seconds, slewing and settling over the next 30 seconds, recording the following 30 seconds of data at the next star position, and so on.

4. WIDE ANGLE EXPERIMENT RESULTS

The pseudo-star is scanned through a grid of 56 or so star positions, more or less uniformly spaced in a 15-degree diameter field of regard. The wide angle scan sequences are designed to begin and end at the center of the field. The scan pattern is shown in Fig. 6. The IIPS pseudo-star positions are shown as black dots. Stars circled in red are the calibrators, forming a nearly-hexagonal pattern (as will the 'grid stars' in the SIM mission). Stars marked with green squares are measured twice; first at the beginning and then again at the end of the scan. They are used to measure the linear time-dependent drift.

The first processing step is to extract the observing part of the data and then to calculate the error between the pathlength from the starlight and from the metrology sensors, as described in section 2.6. Then, for each 30 second observation, the error between starlight and metrology is averaged down to a single number D_{Raw} for each star position (X_i,Y_i). Fig. 8 shows the raw 30 second averages of the error between metrology and starlight in green, versus X and Y star positions. Note that most of the time, the pseudo-star is scanning along columns in the pattern, i.e. Y is varied, as X is held constant. Note the correlation between the raw delay and the star position.

4.1. Linear Time-Dependent Drift Removal

The scan sequence of pseudo-star positions has been designed so that stars number 2 through 6 are each measured a second time after the pattern of target stars is completed (typically about an hour later). These five stars are called 'drift stars' in the remainder of this report. Differences between the first and second measurements of these five drift stars can be used to estimate linear time dependent drift h_{est} over the duration of the experiment. Then, we can remove the linear drift term from the raw measurements in Eq. 2 by subtracting $h_{est}T$ from each measurement. The model equation for the drift-removed delay difference D_{DR} is:

$$D_{DR}(X_i,Y_i) = D_{Raw}(X_i,Y_i,T_i) - h_{est}\,T_i \tag{3}$$

For this run the drift was 0.264 picometers per second. Fig. 9 shows the spatial dependence of the raw delays, after removing linear time-dependent drift. Evidently the field dependence is dominated by a linear (planar) component.

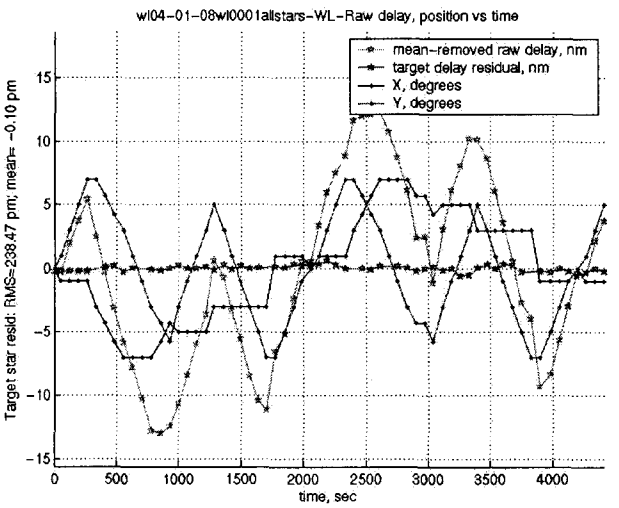

Fig. 8. 30-second integrated delays and star positions versus time.

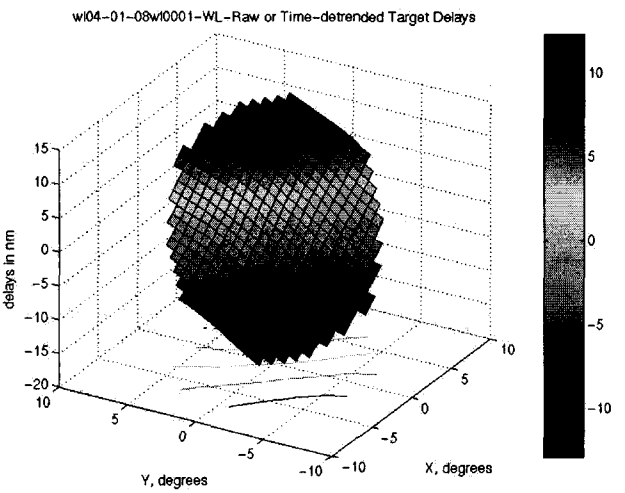

Fig. 9. Spatial dependence of raw target star delays over the wide angle field of regard.

4.2. Systematic Field-Dependent Error Removal

To estimate the first four error terms in Eq. 2, we choose seven calibrator stars arranged in a pattern similar to that of grid stars in a SIM tile. That is, one star at the center of the tile, and six outlying stars at the points of a hexagon concentric with the tile center. We start with a set of measurements of these calibrator stars from which linear time drift has been removed, as in the previous section:

$$D_{CAL}(X_j,Y_j) = a + bX_j + cY_j + d(X_j^2 + Y_j^2) + \varepsilon_j, \tag{4}$$

where now j indexes the calibrator stars. The model parameters a_{est}, b_{est}, c_{est}, and d_{est} are estimated via linear least-squares fit. We estimate the field-dependent bias as:

$$F_{est}(X,Y) = a_{est} + b_{est}X + c_{est}Y + d_{est}\,(X^2 + Y^2) \tag{5}$$

Fig. 10 shows the model surface fitted to the delay measurements of the seven calibrator stars. Though the field dependence is predominantly linear, there is a significant quadratic component as well.

4.3. Single-Tile Delay Measurement Error

Target stars in the field of regards are the 48 or so pseudo-star positions that are not calibrator stars. Again, each target star measurement is corrected for linear time-dependent drift and then for field-dependent errors of the form of Eq. 5 by subtracting the estimated model function F_{est}:

$$D(X_i,Y_i) = D_{DR}(X_i,Y_i) - F_{est}(X_i,Y_i), \tag{6}$$

where D is the corrected white light minus metrology delay measurement. Fig. 11 shows the spatial dependence of the residuals.

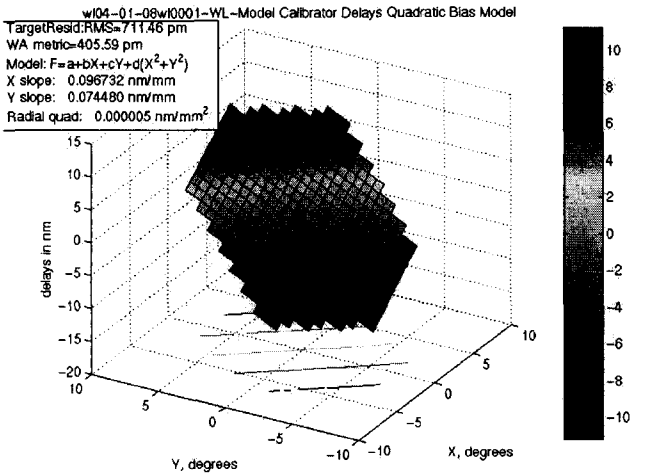

Fig. 10. Fitted model for spatial dependence of target star delays.

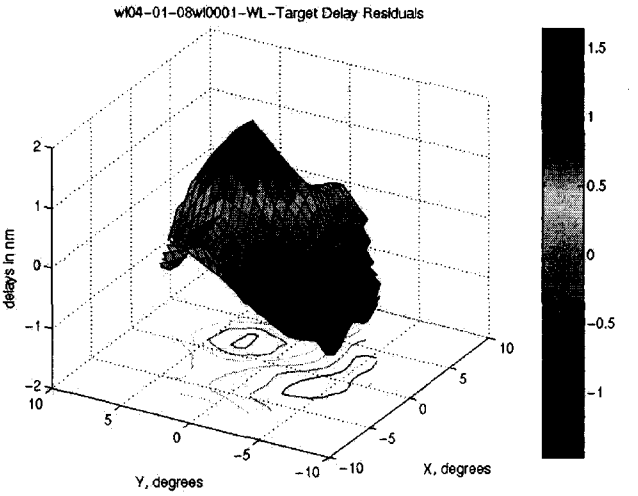

Fig. 11. Spatial dependence of white light versus metrology delay residuals.

The RMS of the residuals of the 48 target star measurements provides a first estimate of the MAM single-tile delay measurement error:

$$\tau = \sqrt{\sum_{k=1}^{M} \frac{D(X_k, Y_k)^2}{M}} \tag{7}$$

where k indexes the target star and M is the number of target stars, and the $D(X_k,Y_k)$ are the corrected white-light minus metrology delay measurements.

4.4. Final Performance Metric

Subtracting the error model of Eq. 5 from the target star delays introduces estimation error into our determination of the MAM single-tile delay measurement error. SIM's error budget is defined as single star error for target stars only, but MAM is making differential measurements, capturing the errors of grid reference and target stars. We can improve the estimate of single measurement delay error by removing this estimation error.

To determine the estimation error, we performed a Monte Carlo simulation (with 10,000 realizations) of a set of stars at the same positions as in our wide angle test sequence. We generated delay measurements of the form of Eq. 2, assuming that the residual single-tile delay measurement error ε is composed of random error σ (RMS) only. The simulation data are then processed using the same linear drift correction and field dependent calibration model as in Eqs. 3-7. We found that the RMS target star delay residual τ was 1.24σ. Note that the multiplier value of 1.24 depends only on the geometry of the pseudo-star locations.

The MAM measurement contains errors from both the inverse-interferometer pseudo-star interferometer and the test-article interferometer. SIM on the other hand will observe perfect stars. We assume that the errors are comparable and contribute equally in quadrature to the single delay measurement error. Therefore, for comparison to the SIM part of the single-tile delay measurement error, we divide by a further factor of $\sqrt{2}$.

Based on the foregoing analysis, we derive the following MAM wide angle performance metric:

$$\Pi = \frac{\tau}{1.24\sqrt{2}} = \frac{1}{1.24\sqrt{2}} \sqrt{\sum_{k=1}^{M} \frac{D(X_k, Y_k)^2}{M}} \tag{8}$$

4.5. Summary Performance for Several Runs

Initial tests were performed with the vertical scan pattern, which uses primarily consecutive vertical (i.e. orthogonal to the direction of delay line motion) moves. To investigate systematics related to scan direction, other scan patterns were tried such as the horizontal pattern that uses primarily horizontal rather than vertical moves.

Nine wide angle test runs were completed with the various scan patterns. Calibration results are collected in Table 1. Fitted quadratic model parameters b, c, and d are quite consistent over these runs.

Table 1. Field dependent calibration parameters.

Run number	b (pm/mm)	c (pm/mm)	d (pm/mm^2)
03-09-29wl0001	98	75	-0.076
03-10-01wl0002	95	71	-0.146
03-10-01wl0003	102	73	-0.060
03-10-02wl0001	111	73	-0.091
03-10-02wl0006	105	76	-0.038
03-10-02wl0007	107	69	-0.089
03-10-02wl0008	102	76	0.003
03-10-08wl0002	99	73	-0.095
03-10-08wl0003	103	75	-0.084

The RMS target star residuals τ and the corresponding performance metric Π for these wide angle runs is presented in Table 2. The performance metric for each of these runs meets SIM's baseline requirement of 1000 picometers for wide angle astrometry and the mean metric approaches the goal performance of 280 picometers.

Table 2. MAM wide angle test performance.

Run number	Target star residuals RMS (picometers)	Performance metric (picometers)
03-09-29wl0001	764	439
03-10-01wl0002	466	268
03-10-01wl0003	585	336
03-10-02wl0001	713	410
03-10-02wl0006	585	336
03-10-02wl0007	550	316
03-10-02wl0008	764	439
03-10-08wl0002	541	311
03-10-08wl0003	578	332

5. NARROW ANGLE EXPERIMENT RESULTS

The goal for MAM was to show agreement between metrology and starlight to 24 pm over the narrow angle field of regard (1 degree).

5.1. Five-star sequence

For the field dependent tests, we used the "Five-star" sequence (Figure 7). The sequence is 30 seconds of observation time at the target star T, followed by 30 seconds to slew to the first reference star R2 and 30 seconds of observation time again. We slew again back to the same target star T, and observe for 30 seconds. Then, we slew to the second reference star R3, we observe for 30 seconds, and slew back to the target star. We continue slewing and observing between the target stars and the other reference stars R4 and R5. Finally, we repeat the sequence from the beginning.

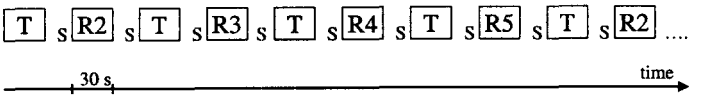

Figure 12 shows the commanded position sent to the IIPS translation motors during the five-star field dependent test. One can see, the four reference stars at +/– 7 mm of IIPS position on each side of the target star.

5.2. Processing the five-star chop sequence

The first processing step is to map the valid part of the data and then to calculate the error between the pathlength from the starlight and from the metrology sensors. Then, for each 30 second observation, the error between starlight and metrology is averaged down to a mean number. Figure 13 shows the 30 second averages of the error between metrology and starlight. The first star in the sequence is the target star. One can see the four reference stars on each side of the target star through their different calibration errors at the nanometer level.

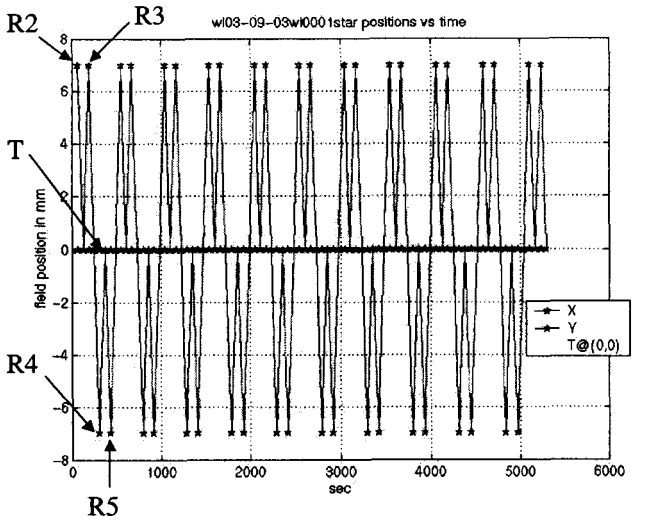

Figure 12 – Commanded position (in millimeters) of the pseudo-star translation actuators during the five-star field dependent test.

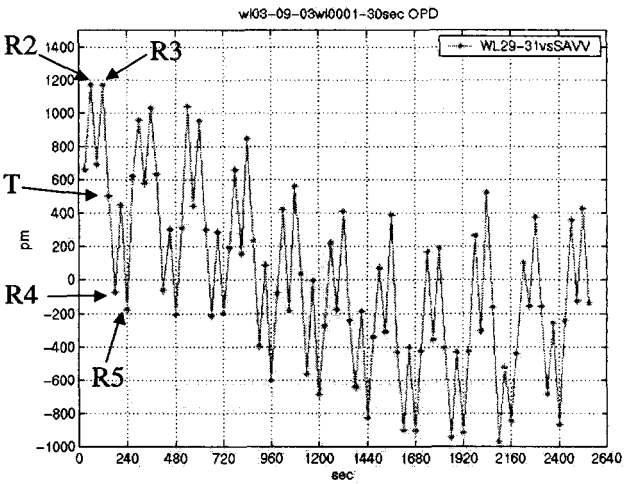

Figure 13 – White light versus metrology OPD for the five-star field dependent test. Each point corresponds to the mean value over the 30 second integration time. The first star of the sequence is the target star.

For each chop, we calculate the difference between the calibration error value at the reference and the target star. Figure 14 presents the narrow angle analysis of the data based on the SIM observation scenario. $\overline{T}$ and $\overline{R}_i$ are the mean optical differences between the metrology and starlight paths for each 30 second integration for the target or one of the four reference stars, respectively. We calculate the second difference of the $\overline{T}$ and $\overline{R}_i$ values in order to estimate the mean field dependent metrics from the target to the reference D_{Ri}. A full MAM-chop includes four reference stars, one on each side of the target (up, down, left and right). ε_i is the error in the measurement of the position of the target star relative to the four reference star frame for one chop sequence i. Finally, we combined the ε_i chops together to reduce the random contribution and improve the results.

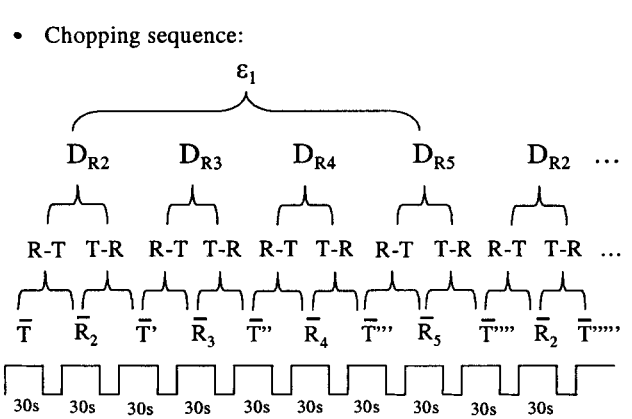

• Single "TRT" chop (<.,.,.,.> is the mean operator):

$$D_{R2} = \langle (\bar{R}_2 - \bar{T}) , (\bar{R}_2 - \bar{T}') \rangle = \bar{R}_2 - \langle \bar{T}, \bar{T}' \rangle$$

$$D_{R3} = \langle (\bar{R}_3 - \bar{T}') , (\bar{R}_3 - \bar{T}'') \rangle = \bar{R}_3 - \langle \bar{T}', \bar{T}'' \rangle$$

....

• Multiple star chop:

$$\varepsilon = \langle D_{R2} , D_{R3} , D_{R4} , D_{R5} \rangle$$

$$\varepsilon = \langle (\bar{R}_2 - \langle \bar{T}, \bar{T}' \rangle) , \ldots , (\bar{R}_5 - \langle \bar{T}''', \bar{T}'''' \rangle) \rangle$$

$$\varepsilon = \langle \bar{R}_2, \bar{R}_3, \bar{R}_4, \bar{R}_5 \rangle - \langle \bar{T}, \bar{T}, \bar{T}', \bar{T}'', \bar{T}'', \bar{T}''', \bar{T}''', \bar{T}'''' \rangle$$

Figure 14 – Calculation of the error metrics for the five-star field dependent sequence, based on the SIM observation scenario.

Figure 15 shows the field dependent offsets D_{Ri} between the target and each reference star. The offsets for the first and third reference stars (horizontal pair) are at about +/– 0.5 nm, and the offsets for the second and fourth reference stars (vertical pair) are at about +/– 0.6 nm. In fact, we expect the two calibration offsets for a given pair of stars to be mostly opposite since the two reference stars are located exactly in opposite directions from the target star. On the other hand, there is no specific reason for the mean offsets for the vertical pair and horizontal pair to be similar. The mean value of the four calibration offsets ε is the error of the measured process plus the non-linear portion of the calibration curve. In this test, that non-linear portion is very close to zero, since the calibration curve is very linear in the narrow angle field of regard of MAM (+/–0.5 degree).

5.3. Field dependent test results

Figure 16 shows the rms error of the linear calibration (middle curve of Figure 15) as a function of the number of chopped values averaged together. In the SIM scenario, the target star is observed 10 times, but MAM observes the reference stars four at a time. This limits the numbers of chops averaged together to 4, 8 or 12 chops. Therefore the final metric for MAM is the mean between the rms error for the 8-chop and 12-chop averages. From Figure 16, we measure 24 picometers rms calibration accuracy of the MAM interferometer over its narrow field of regard. Again, a ½ correction is applied to the MAM numbers to be mapped to SIM's performance error budget. From Figure 16, the accuracy of the TA alone for the target star only would be 12 pm over the narrow angle field of regard, significantly below the 24 pm requirement for 1 micro-arcsecond narrow angle astrometry.

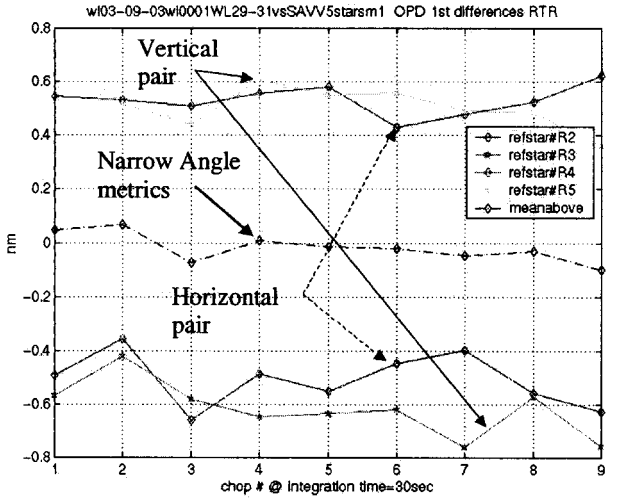

Figure 15 – Position of the four reference stars relative to the target star in terms of error between starlight and metrology for the field dependent test. One can see +/-0.5 nm field dependent bias between the target and each reference star.

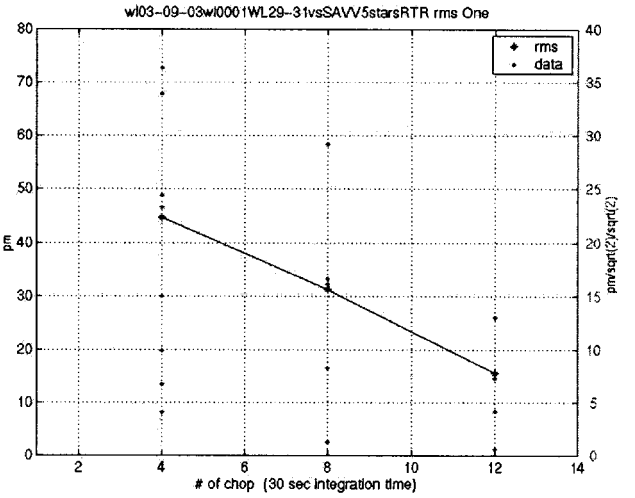

Figure 16 – Error between white light and metrology paths as a function of the number of chops averaged together for the field dependent test using the narrow angle chopping analysis.

5.4. Performance Metrics

A correction must be applied to map MAM's performance numbers to SIM's performance error budget: MAM errors include both the inverse interferometer pseudo-star and the test article interferometer contribution. SIM on the other hand will observe perfect stars. Also, SIM's error budget is defined as single star error for the target star, but MAM is making differential measurements, capturing the errors of reference and target stars. If the residual error is assumed random, then the error could be evenly split between IIPS and TA, and between the target and reference stars. A factor of 1/2 is applied to accommodate for the extra error[1]. For example, a 24 pm error on a narrow angle measurement on MAM would map into a 12 pm performance of the SIM instrument.

Figure 17 shows the performance of the field dependent test for a 2-week period. Each point on the graph corresponds to a separate 90-minute 5-star run. For each run, the data were processed as previously described and the 8-chop and 12-chop rms values were averaged to a single performance number. The corresponding mean performance for SIM is 20.2 pm below the 24 picometer goal level for the Science interferometer. In fact, 75% of the runs are below the SIM goal level.

[1] $1/2 = 1/\sqrt{2} \cdot 1/\sqrt{2}$, each $1/\sqrt{2}$ factor corresponds to half of the error in the root mean sum sense.

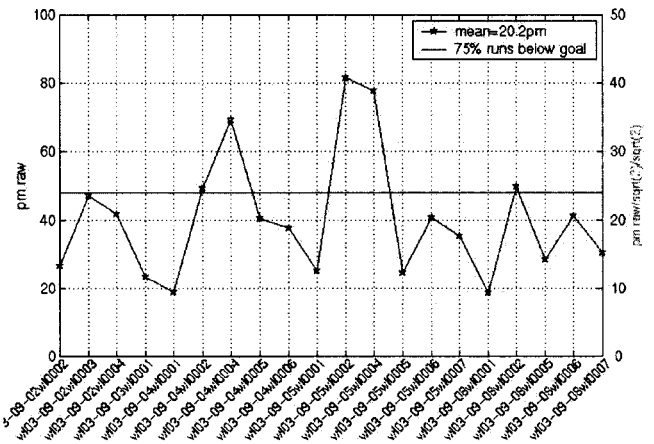

Figure 17 – Performance of several 5-star field dependent runs for the September 2003 period. The left scale shows raw MAM performance numbers in picometers rms as previously described. The right scale shows the corresponding SIM performance accounting the difference between the two experiments. The mean performance is below the goal level (horizontal line).

6. CONCLUSION

We have described how SIM will process wide angle astrometric data, how the MAM testbed is used to validate the approach and how it captures most of the measurement errors. We have shown MAM performance data around 350 pm rms for the wide angle field dependent tests. The achieved performance validates SIM's baseline performance of 10 micro-arcsecond, while approaching the goal target of 4 micro-arcsecond astrometry. A recent deeper study of the residual errors shows that the performance is currently limited by systematic field dependent errors that could be further calibrated. Then we have shown MAM performance data of 40 pm rms for the narrow angle field dependent tests. The achieved performance maps to 20 picometers rms for SIM's science interferometer, below the goal level that enable single micro-arcsecond astrometry.

ACKNOWLEDGEMENTS

The research described in this publication was performed at the Jet Propulsion Laboratory of the California Institute of Technology, under contract with the National Aeronautics and Space Administration. The authors would like to thank the entire MAM team for its contribution to the success of the experiment.

REFERENCES

1. M. Shao, "Overview of SIM", *SPIE Conf. on New Frontiers in Stellar Interferometry*, vol. 5491, 2004.

2. G.W. Neat, James W. Melody, and B.J. Lurie, "Vibration Attenuation Approach for Spaceborne Optical Interferometers", *IEEE Transactions on Control System Technology*, vol. 6, no. 6, Nov. 1998.

3. R. Goullioud, O. S. Alvarez-Salazar, and B. Nemati, "Dim star fringe stabilization demonstration using pathlength feed-forward on the SIM Testbed 3 (STB3)", *SPIE Conf. on Interferometry in Space*, vol. 4852, 2002.

4. O. S. Alvarez-Salazar, R. Goullioud, and A. Azizi, "SIM system testbed: 3-baseline stellar interferometer on a 9-meter long flexible structure", *SPIE Conf. on New Frontiers in Stellar Interferometry*, vol. 5491, 2004.

5. F. G. Dekens, "Kite: status if the external metrology system testbed for SIM", *SPIE Conf. on New Frontiers in Stellar Interferometry*, vol. 5491, 2004.

6. R. Goullioud and T. J. Shen, "SIM astrometric demonstration at 24 picometers on the MAM testbed", *IEEE Aerospace Conference*, Big Sky, MT, 2004.

7. R. Goullioud and T. J. Shen, "MAM testbed detail description and alignment", *IEEE Aerospace Conference*, Big Sky, MT, 2004.

8. F. Zhao, R. Diaz, G. M. Kuan, N. Sigrist, Y. Beregovski, L. L. Ames, K. Dutta, "Internal metrology beam launcher development for the space interferometry mission," *SPIE conference on Interferometry in Space*, vol. 4852, 2002.

9. M. W. Regehr, B. Hines and B. Holmes, "Optical Path Control in the MAM Testbed", *IEEE Aerospace Conference*, Big Sky, MT, 2003.

10. Y. Gürsel, "Very high-precision absolute surface gauges for building and qualifying SIM testbed interferometer compound optics", *SPIE conference on Interferometry in Space*, vol. 4852, 2002.